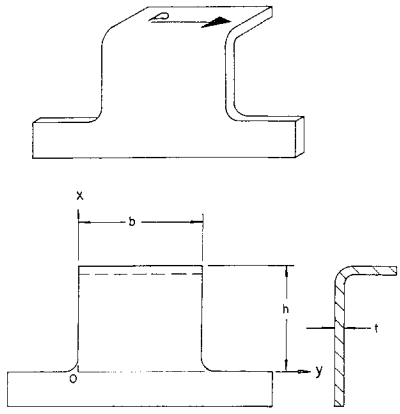

Fig 1 Coordinate system and typical castellation

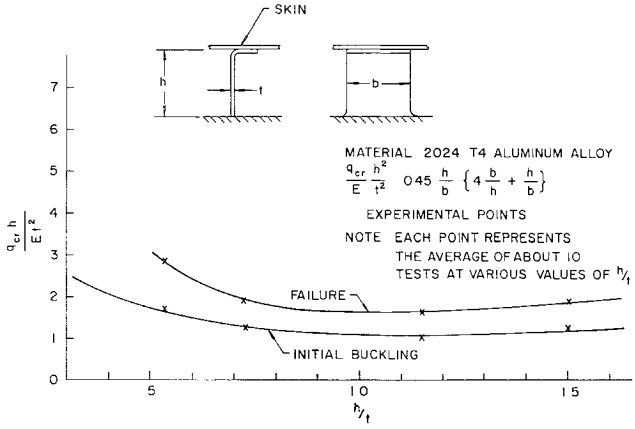

Fig 2 Comparison of theoretical and experimental results

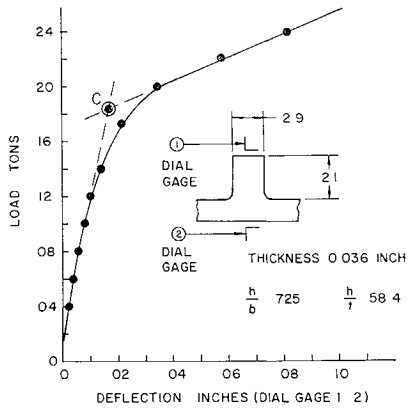

Fig 3 Typical load-deflection curves from Ref 2

The strain energy and the work done by the external forces now follow from the equations

$$V = \frac{1D}{2}\int_0^b\int_0^h \left\{\left[\frac{\partial^2 w}{\partial x^2}+\frac{\partial^2 w}{\partial y^2}\right]^2 - 2(1-\nu)\left[\frac{\partial^2 w}{\partial x^2}\frac{\partial^2 w}{\partial y^2}-\left(\frac{\partial^2 w}{\partial x \partial y}\right)^2\right]\right\} dx\,dy \quad (2)$$

and

$$T = \frac{1}{2}\int_0^b\int_0^h \left\{N_x\left(\frac{\partial w}{\partial x}\right)^2 + 2N_{xy}\frac{\partial w}{\partial x}\frac{\partial w}{\partial y}\right\} dx\,dy \quad (3)$$

where $D = Et^3/12(1-\nu^2)$, and all other symbols have their customary meaning In Eq (3) we require some knowledge of the direct and shear forces, N_x and N_{xy}, respectively A reasonable distribution is given by

$$N_x = (Pt/I)(xy - \tfrac{1}{2}bx) \quad (4)$$

and

$$N_{xy} = \tfrac{3}{2}(P/b^3)(b^2 - y^2) \quad (5)$$

Upon su bstitution, we obtain the critical shear stress q_c :

$$\frac{q_{cr}h^2}{Et^2} = 0\,045\,\frac{h}{b}\left\{4\frac{b}{h}+\frac{h}{b}\right\}^2 \quad (6)$$

This relationship is compared in Fig 2 with test results obtained from Ref 2 A typical load-deflection curve is shown in Fig 3 The point of intersection C of the initial and final slopes of the load deflection curve is assumed to determine the critical buckling load and is chosen for comparison with theoretical results Clearly, our analysis is restricted to stress levels at which plasticity does not play a dominant role

References

[1] "Strength of castellations in shear," Roy Aeronaut Soc Data Sheet 02 03 24, London (November 1949)

[2] Fenn, E E, "Further tests on castellation teeth "Internal Rept C R 586, Bristol Aeroplane Co, Ltd, Bristol, England (November 1949)

Calculation of Cylindrical Blast Wave Propagation with Counterpressure

BERNARD STEGINSKY*
Battelle Memorial Institute, Columbus, Ohio

Nomenclature

- a_∞ = speed of sound in undisturbed gas
- C_D = drag coefficient
- d = diameter of cylinder
- E = explosion energy per unit length of charge or drag of equivalent body in hypersonic flight
- m = Lagrangian variable, $\rho_\infty R^2/2$
- M = Mach number, u_∞/a_∞
- p_∞ = pressure of undisturbed gas
- p_s = pressure behind shock wave
- p_p = pressure at piston surface
- q = $a_\infty{}^2/\dot{R}_0{}^2$
- R = shock wave coordinate at time when gas particle crosses shock wave
- R_0 = shock-wave coordinate at any time
- R_p = coordinate of piston surface at any time
- t = time
- u_∞ = velocity of undisturbed gas with respect to observer fixed in body frame in equivalent hypersonic flight problem
- x = axial distance in equivalent hypersonic flow problem
- γ = ratio of specific heats
- ϵ = $(\gamma-1)/(\gamma+1)$
- ρ_∞ = density of undisturbed gas
- ρ_s = density behind shock wave

WE propose to show how the integral method of Chernyi[1] may be used to furnish a second approximation to the shock-wave shape and pressure predicted by cylindrical blast-wave theory [2] The comparative ease with which the result is obtained, and the good agreement with experiment, affords an excellent illustration of the potential value of this powerful yet simple method in the analysis of hypersonic flows

The starting point in our analysis is the simplified version of the energy-integral equation for the problem of a violent explosion due to a line charge, followed by the expansion of a

Received November 1, 1963

* Research Aerodynamicist, Fluid and Thermal Mechanics Research Group

cylindrical piston originating from the line of symmetry:

$$\frac{\pi}{2}\rho_\infty R_0^2\left(\frac{\partial R}{\partial t}\right)^2+\frac{\pi}{\gamma-1}(R_0^2-R_p^2)p_p= E+\frac{\pi R_0^2}{\gamma-1}p_\infty+2\pi\int_0^t p_pR_p\dot{R}_p dt \quad (1)$$

This equation is derived in Ref 1 from the conservation-of-energy equation by assuming that the entire mass of gas in the disturbed region is concentrated in a negligibly thin layer just behind the shock wave, and that the pressure, although changing rapidly in this layer, is constant throughout the remainder of the shocked region Thus, $\partial R/\partial t$ corresponds to the gas-particle velocity at the shock wave which is taken to be[1]

$$\frac{\partial R}{\partial t}=\frac{2}{\gamma+1}\left(\dot{R}_0-\frac{a_\infty^2}{\dot{R}_0}\right) \quad (2)$$

For the pressure we shall require only that the expression used in conjunction with the energy equation satisfy the momentum equation to $0(\epsilon)$ but agree with the boundary condition on the shock wave The pressure is found easily from these conditions to be†

$$p=\frac{2}{\gamma+1}\rho_\infty\dot{R}_0^2+\frac{1}{2}\rho_\infty R_0\ddot{R}_0\left(1-\frac{R^2}{R_0^2}\right)-\frac{\gamma-1}{\gamma+1}p_\infty \quad (3)$$

In Table 1 a numerical comparison is made between values of

Table 1 Values of p_p/p_s on power-law bodies as computed from similarity theory and from Eq (3)

n	Similarity solution[1]	Equation (3)
1 0	1 0497	1 0
0 9	0 982	0 933
0 8	0 891	0 850
0 7	0 780	0 743
0 5	0 3729	0 4

(p_p/p_s) calculated from Eq (3) and the exact values obtained from similarity theory for $p_\infty = 0$ The numerical values correspond to the special class of bodies called power-law bodies which are characterized by shock-wave shapes of the form $R_0 = Ct^n$ where $\frac{1}{2} < n \leq 1$ The special case $n = \frac{1}{2}$ is singular and corresponds to the problem of a violent explosion It is seen that the agreement between the values obtained from the approximate theory and those obtained from exact numerical computation is rather good and quite satisfactory for our purposes

Equation (1) may be specialized to the case of a violent explosion simply by setting $R_p = 0$ ‡ Let us point out that the approximation that led to the derivation of Eqs (1) and (3) presupposes a strong compression such that the density ratio ρ_∞/ρ is small This ratio may be written

$$(\rho_\infty/\rho_s)=\epsilon+[2/(\gamma+1)]q \quad (4)$$

We infer from Eq (4) and the preceding that we must regard q as well as ϵ as a small parameter in the theory

In solving Eq (1) we shall take into account first-order terms in the parameters ϵ and q § This means that we can neglect in Eqs (2) and (3) those terms which, when substituted in Eq (1), give rise to terms of order ϵ^2, q^2, ϵq, and higher with respect to those retained Carrying out the indicated substitutions and approximations, we obtain the following equation for $R_0(t)$:

$$\frac{\pi}{2}\left(\frac{2}{\gamma+1}\right)^2\rho_\infty R_0^2\dot{R}_0^2+\frac{\pi}{\gamma-1}\rho_\infty R_0^2\left(\frac{2}{\gamma+1}\dot{R}_0^2+\frac{1}{2}R_0\ddot{R}_0\right)= E+\frac{\pi}{\gamma-1}p_\infty R_0^2+\text{higher order terms} \quad (5)$$

Equation (5) possesses an exact analytic solution for $R_0(t)$:

$$R_0(t)=f_1(\gamma)\left(\frac{8E}{\pi\rho_\infty}\right)^{1/4}t^{1/2}\left\{1+f_2(\gamma)\frac{a_\infty^2}{(8E/\pi\rho_\infty)^{1/2}}t\right\}^{1/2} \quad (6)$$

where

$$f_1(\gamma)=\left[\frac{(\gamma-1)(\gamma+1)^2}{6\gamma-\gamma^2-1}\right]^{1/4}$$

and

$$f_2(\gamma)=\left[\frac{\gamma+1}{2\gamma f_1(\gamma)}\right]^2$$

To bring Eq (6) into a form which is convenient for application to hypersonic flows, we make the following correspondence between the explosion problem and its aerodynamic analogue (equivalence principle):

$$t\rightarrow(x/u_\infty) \qquad E\rightarrow(\pi d^2/8)\rho_\infty u_\infty^2 C_D \quad (7)$$

The correspondence is made complete by assuming that the body associated with the flow is any unyawed slender object having a blunt nose [3] Hence, d and C_D correspond to the transverse dimension and drag coefficient, respectively, of the nose For definiteness, we take the body to consist of a hemispherical nose with a cylindrical afterbody ¶

Making the above substitutions in Eq (6) we obtain

$$\frac{R_0}{d}=f_1(\gamma)C_D^{1/4}\left(\frac{x}{d}\right)^{1/2}\left\{1+\frac{f_2(\gamma)}{M^2C_D^{1/2}}\frac{x}{d}\right\}^{1/2} \quad (8)$$

The pressure distribution on the axis is obtained from Eq (3) and takes the following form:

$$\frac{p}{p_\infty}=\frac{f_3(\gamma)M^2C_D^{1/2}}{\frac{x}{d}\left\{1+[f_2(\gamma)/M^2C_D^{1/2}]\frac{x}{d}\right\}}+f_4(\gamma) \quad (9)$$

where

$$f_3(\gamma)=\frac{\gamma(3-\gamma)}{8(\gamma+1)}[f_1(\gamma)]^2$$

$$f_4(\gamma)=\frac{\gamma+1}{2\gamma}-\frac{\gamma-1}{\gamma+1}$$

† The pressure may be shown to satisfy the momentum equation $\ddot{R}_0 = -R_0\,\partial p/\partial m + 0(\epsilon)$ by direct substitution of (3); it is also easily verified that (3) has the correct form at the shock wave $(R = R_0)$

‡ In this case p_p in Eq (1) corresponds to the pressure on the axis of symmetry

§ The case of $q = 0$ corresponds to the blast-wave problem without counterpressure so that the retention of terms of $0(q)$ will yield a second approximation to the blast-wave problem

¶ For this choice of body shape, R_p is not 0 but equal to $\frac{1}{2}d$ Strictly speaking, we should not have neglected the effect of finite piston radius in the second term on the left-hand side of Eq (1) However, the error we incurred by omitting it is small except for $t \rightarrow 0$, where the equivalence principle does not apply anyway

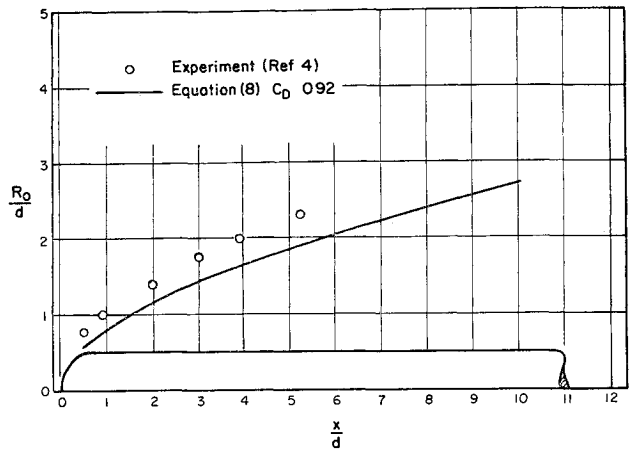

Fig 1 Shock shape for hemisphere-cylinder at Mach no 7 7 ($\gamma = \frac{7}{5}$)

The values of f_1 f_2, f_3, and f_4 for monatomic ($\gamma = \frac{5}{3}$) and diatomic ($\gamma = \frac{7}{5}$) gases are given in Table 2

The results of the present analysis, embodied in Eqs (8) and (9), are compared with experimental data[4] on hemisphere-cylinder combinations in Figs 1–4 The experiments at $M =$ 7 7 were performed in air whereas those at the higher Mach numbers were carried out in helium It is seen that the agreement with experiment is better at the higher Mach numbers This improvement in the theory for increasing Mach numbers

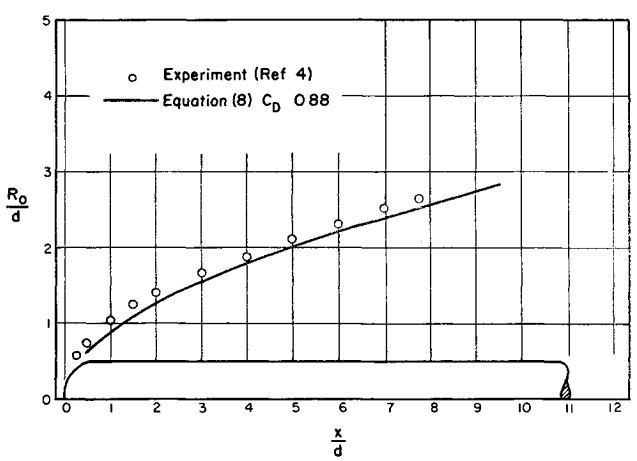

Fig 2 Shock shape for hemisphere-cylinder at Mach no 21 ($\gamma = \frac{5}{3}$)

is entirely consistent with the nature of the approximations concerning the structure of the shock layer

It is believed that the method just presented for calculating the shock-wave shape and pressure distribution over a body in hypersonic flow has the following distinct advantages over more exact but complicated numerical methods:

1) Equations (1–3) may be used to determine the shock-wave shape and pressure distribution over unyawed slender bodies of general shape with or without nose blunting in a simple, direct fashion

2) The explicit appearance of the Lagrangian coordinate R in Eq (3) makes the method ideally suited for use in conjunction with an integration scheme such as the streamtube method[5] for analyzing real gas effects in hypersonic flows

3) The appealing simplicity of the method suggests its use as an analytical tool in obtaining first approximations to unsolved flow problems such as, for example, the inviscid flow in the near-wake region behind a body in hypersonic flight

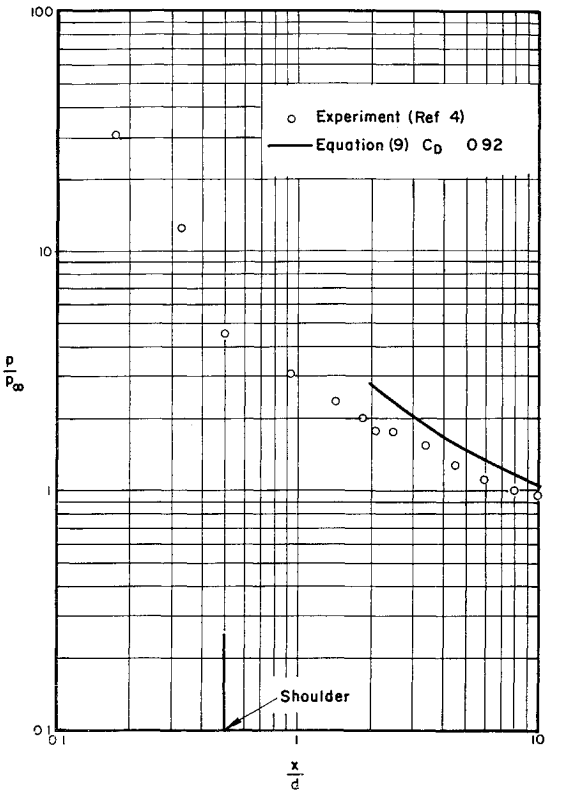

Fig 3 Pressure on hemisphere-cylinder at Mach no 7 7 ($\gamma = \frac{7}{5}$)

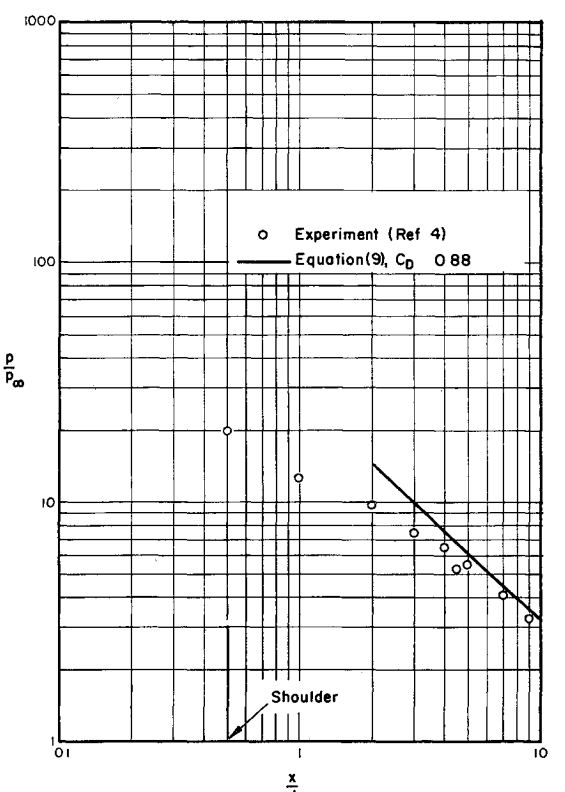

Fig 4 Pressure on hemisphere-cylinder at Mach no 18 1 ($\gamma = \frac{5}{3}$)

References

[1] Chernyi, G G , *Introduction to Hypersonic Flow* (Academic Press, Inc , New York, 1961), Chap V pp 201 ff 219 86–87, 216

[2] Sedov, L I, *Similarity and Dimensional Methods in Mechanics* (Academic Press, Inc, New York, 1959), Chap IV, pp 210 ff

[3] Lees, L and Kubota, T, 'Inviscid hypersonic flow over blunt-nosed slender bodies," J Aeronaut Sci **24**, 195–202 (1957)

[4] Van Hise, V, "Analytic study of induced pressure on long bodies of revolution with varying nose bluntness at hypersonic speeds," NASA TR R-78 (1960)

[5] Lin, S C and Teare, J D, "A streamtube approximation for calculation of reaction rates in the inviscid flow field of hypersonic objects" Avco Everett Res Lab Res Note 223 (August 1961)

Contours for Stagnation-Point Mass Injection in Hypersonic Flow

CHANG-YI WANG*
Massachusetts Institute of Technology, Cambridge, Mass

A RECENT investigation[1] demonstrated the possibility of achieving well-defined blunt contact surfaces ahead of a rounded central injection port exhausting upstream into the shock layer Advantageously, there results a rather large and inviscid buffer layer of injected fluid precisely in the region of most severe thermal heating problems This note arises as a result of interest in generalizing the analysis to a wider class of blunted shapes, in particular to slender bodies that may require thermal protection at the nose [2]

Figure 1 shows schematically a contoured injection port and a contact surface established between the external (shock) layer and the internal (buffer) layer For a hemispherical contact surface, the solutions of Li and Geiger[3] are reasonable approximations for the contour [1] More generally, one may introduce an axisymmetric conical coordinate system[4] in which continuity permits the definition of a stream function ψ such that

$$\frac{\partial\psi}{\partial\eta} = \xi\eta\left(\frac{C\xi^2+\eta^2}{C+B\eta^2}\right)^{1/2}\rho q_{(\xi)}$$
$$\frac{\partial\psi}{\partial\xi} = -\xi\eta\left(\frac{C\xi^2+\eta^2}{1-B\xi^2}\right)^{1/2}\rho q_{(\eta)} \qquad (1)$$

and the momentum equation takes the form

$$\frac{\partial}{\partial\xi}\left\{\frac{\nabla\times\bar{q}}{\rho\xi\eta}\frac{\partial\psi}{\partial\eta}\right\} - \frac{\partial}{\partial\eta}\left\{\frac{\nabla\times\bar{q}}{\rho\xi\eta}\frac{\partial\psi}{\partial\xi}\right\} = 0 \qquad (2)$$

Here $q_{(\xi)}$ and $q_{(\eta)}$ are the components of $\bar{q}$, B and C $(= 1 - B)$ are bluntness parameters, and the Cartesian coordinate description follows from

$$x = B^{-1}\{1 - [(1-B\xi^2)(C+B\eta^2)]^{1/2}\} \qquad y = \xi\eta \quad (3)$$

Since Eq (2) implies that $(\nabla\times\bar{q})/\rho\xi\eta$ is some function of ψ, say $f(\psi)$, it follows that

$$\frac{(1-B\xi^2)^{1/2}}{\rho\eta^2\xi}\frac{\partial}{\partial\xi}\left[\frac{(1-B\xi^2)^{1/2}}{\rho\xi}\frac{\partial\psi}{\partial\xi}\right] + \frac{(C+B\eta^2)^{1/2}}{\rho\eta\xi^2}\frac{\partial}{\partial\eta}\left[\frac{(C+B\eta^2)^{1/2}}{\rho\eta}\frac{\partial\psi}{\partial\eta}\right] = -(C\xi^2+\eta^2)f(\psi) \quad (4)$$

Further simplifications follow from introducing $\mu = (1 - B\xi^2)^{1/2}/B$ and $\nu = (C + B\eta^2)^{1/2}/B$ in place of (ξ and η), so that Eq (4) becomes

$$\eta^{-2}\frac{\partial}{\partial\mu}\left(\frac{1}{\rho}\frac{\partial\psi}{\partial\mu}\right) + \xi^{-2}\frac{\partial}{\partial\nu}\left(\frac{1}{\rho}\frac{\partial\psi}{\partial\nu}\right) = \rho B(C\mu^2 - \nu^2)f(\psi) \qquad (5)$$

An irrotational ($f = 0$), constant-density flow within a spherical ($B = 1$) boundary then implies

$$(1-\mu^2)\psi_{\mu\mu} + \nu^2\psi_{\nu\nu} = 0 \qquad (6)$$

By separating variables, letting $\psi = M(\mu)N(\nu)$, we find that $M(\mu)$, in general, is a hypergeometric function with degenerate cases and that $N(\nu)$ is in the form of $C_1\nu^{-m} + C_2\nu^{m+1}$ The boundary conditions are $q_{(\eta)}|_{\eta=1} = 0$, and $q_{(\xi)}|_{\eta=1}$ equals the corresponding velocity for Newtonian pressure distribution These are satisfied exactly by

$$\psi = \frac{2}{3}\left(\frac{\rho\rho_\infty V_\infty^2}{2}\right)^{1/2}\xi^2\left(\frac{1}{\eta} - \eta^2\right) \qquad (7)$$

where ρ_∞, V_∞ refer to freestream values (see Fig 2)

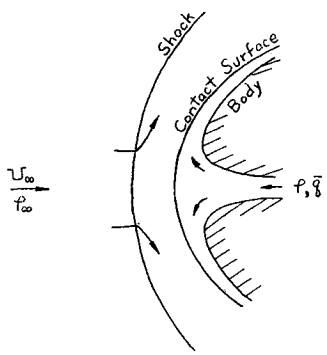

Fig 1 Schematic diagram

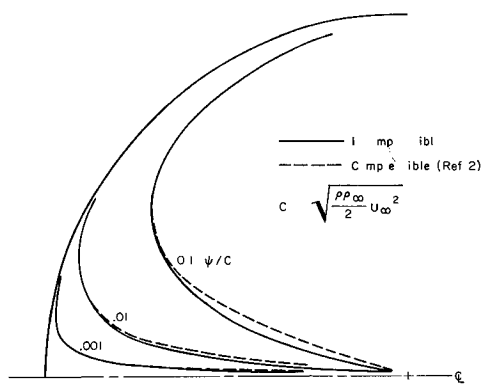

Fig 2 "Inner" streamlines for spherical contact surface with Newtonian pressure

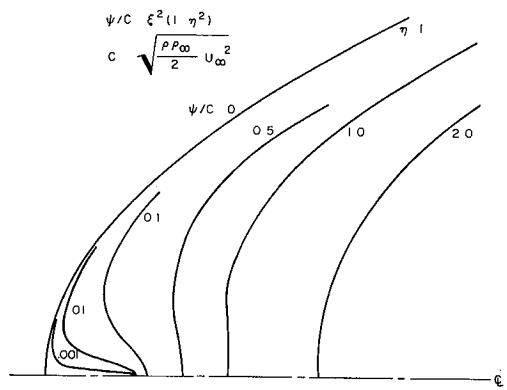

Fig 3 "Inner" streamlines for paraboloidal contact surface with Newtonian pressure

Received October 29, 1963 This research investigation was supported in part by the U S Air Force under Contract No AF 49(638)-245 The author wishes to offer sincere thanks to Judson R Baron for his initiation and guidance for the work on this subject

* Research Assistant, Department of Aeronautics and Astronautics